Materials Research Bulletin 68 (2015) 234–239

Contents lists available at ScienceDirect

Materials Research Bulletin

journal homepage: www.elsevier.com/locate/matresbu

Graphene nanosheets decorated with tunable magnetic nanoparticles and their efficiency of wastewater treatment

Yao Wu [a], Zhiming Li [b], Jie Chen [a], Chenguang Yu [a], Xiao Huang [a], Cuizhen Zhao [a], Lianfeng Duan [a], Yue Yang [a], Wei Lü [a,*]

[a] Key Laboratory of Advanced Structural Materials, Ministry of Education, Changchun University of Technology, Changchun 130012, China
[b] State Key Laboratory of Luminescence and Applications, Changchun Institute of Optics, Mechanics and Physics, Chinese Academy of Sciences, Changchun 130033, China

ARTICLE INFO

Article history:
Received 21 July 2014
Received in revised form 3 January 2015
Accepted 31 March 2015
Available online 1 April 2015

Keywords:
A. Nanostructures
B. Chemical synthesis
B. Magnetic structure

ABSTRACT

Magnetic graphene–Fe_3O_4 nanocomposites (G/Fe_3O_4) were fabricated by a facile and fast one-pot method and used as adsorbent to remove dye for wastewater using Rhodamine B as the adsorbate. Samples with different weight ratios of graphene oxide (GO) to Fe_3O_4 were prepared. The transmission electron microscopy results exhibit that the sizes of Fe_3O_4 nanocrystals decrease with the increasing of weight ratio of GO to Fe_3O_4. The magnetic characterization demonstrates that the saturation magnetization of nanocomposites decreases with the decreasing sizes of Fe_3O_4 nanocrystals. The investigation of adsorption kinetics and isotherm indicates the adsorption process can be described by Langmuir model and nanocomposites with the smaller sizes of Fe_3O_4 nanoparticles show better adsorption ability. Furthermore, the adsorbents could be recovered conveniently by magnetic separation and recyclable used after desorption process, and the decline in efficiencies of all samples is not more than 1.5% after five cycling runs.

1. Introduction

Graphene as a two-dimensional carbon material with unique electrical, mechanical, thermal, optical properties and huge theoretical specific area has received intense interest in various fields [1–6]. Graphene oxide (GO) is a precursor of graphene with oxygen-containing functional groups on the basal plane and the sheet edge and it exhibits good performance [7]. The tunable oxygen functional groups of GO facilitate surface modifications and make it a promising material of preparation [8]. Due to the increasing importantance of wastewater treatment, the potential application of graphene/Fe3O4 nanocomposites in wastewater treatment had attracted extremely interested.

Up to now, various metal oxides such as TiO_2, MnO_2, ZnO, Fe_2O_3, Fe_3O_4 and CuO have been reported to modify graphene nanosheets. Among them, magnetic nanoparticles, especially Fe_3O_4 nanocrystals (NCs) have attracted a large number of investigations in recent years due to their excellent magnetic properties, chemical stability, non-toxicity, and low magnetocrystalline anisotropy [9–14]. Recently, the preparation of graphene/Fe_3O_4 nanocomposites (G/Fe_3O_4) has been reported, and they have potential applications in drug delivery, energy storage, and removal of contaminants from wastewater [15–18]. Because of water pollution has become increasingly important, the potential application in wastewater treatment had attracted extremely interested. Compared with others methods for the removal of organic pollutants and heavy metal ions, such as chemical oxidation [19], membrane filtration [20], ion exchange [21], photocatalytic degradation [22], the G/Fe_3O_4 nanocomposites as adsorbent for wastewater treatment have many advantages including high absorption efficiency, separation convenience, recyclability, eco-friend [23].

Anchoring Fe_3O_4 NCs on the surface of functionalized graphene nanosheets could not only combine the separation convenience of the magnetic materials and high adsorption capacity of graphene, but also provide additional novel properties due to the interaction between the Fe_3O_4 NCs and graphene. Graphene with large surface could not only avoid the aggregation and growth of the magnetic NCs, often resulting in a special magnetic character, but also increase the adsorption capacity and enhance the dispersity of the composites. G/Fe_3O_4 nanocomposites with different properties were prepared by some groups [24–28]. However the preparation methods are generally multistep, hard to control and they also require some rigorous conditions, and the relationship between

* Corresponding author. Tel.: +86 431 85716421; fax: +86 431 85716426.
E-mail address: lw771119@hotmail.com (W. Lü).

http://dx.doi.org/10.1016/j.materresbull.2015.03.073
0025-5408/

G/Fe_3O_4 ratio in the composites and their efficiency of extraction of dye from aqueous solution is undefined. According to previous reports [15–18,24–48] for preparation of G/Fe_3O_4, the synthesis generally involved hydrothermal or coprecipitation methods at temperature in the range of 70–200 °C followed by calcinations at temperature in the range of 400–550 °C in protective atmosphere. Herein, we synthesized G/Fe_3O_4 nanocomposites by an efficient method at low reaction temperature. In order to study the balance between magnetic and absorption of the nanocomposites, we tuned the loading amount of Fe_3O_4 NCs by controlling the weight ratio of GO to Fe_3O_4 NCs. Furthermore, adsorption kinetics and adsorption isotherms were investigated for researching sorption mechanisms of G/Fe_3O_4. It is found that size and magnetization of Fe_3O_4 NCs decrease with the decreasing amount of Fe_3O_4 in hybrid composite, whereas absorbing capacity was improved. Adsorption kinetics and adsorption isotherms suggest that the adsorption of organic dyes by G/Fe_3O_4 was regarded as physical adsorption combined with effect of chemical adsorption.

2. Experiments

2.1. Chemicals

Iron(III) chloride hexahydrate, iron(II) chloride tetrahydrate, hydrazine hydrate, PDDA (MW100,000–200,000), and Rhodamine B (Rh.B) were purchased from Aladdin. All other chemicals were of analytical grade. Water used in all experiments was doubly distilled and purified by a Milli-Qsystem.

2.2. Characterization

Transmission electron microscopy (TEM) images were obtained using a JEOL2010 transmission electron microscopy. The powder X-ray diffraction (XRD) measurements were performed using a D-MAX IIA X-ray diffractometer with CuKa radiation (λ = 1.5406 Å). The concentrations of dye solutions were measured using UV-2501 spectrophotometer. The magnetic properties were measured by a vibrating sample magnetometer (VSM lakeshore7407) at room temperature. The Ms (emu/g) was measured by moment/mass (emu/g) at 16 kOe.

2.3. Synthesis of G/Fe_3O_4 nanocomposites

GO was synthesized from natural graphite powder (spectral requirement, Shanghai Chemicals, China) according to a modified Hummers method [29]. The resulting purified GO powders were collected by centrifugation and air drying at room temperature. The G/Fe_3O_4 nanocomposites were prepared according to our previous report [30]. Typically, a solution including 5 mg GO was prepared and stirred 15 min, and 500 μl PDDA (20 wt%) was added followed by 30 min stirring. Subsequently, $FeCl_3{\cdot}6H_2O$ and $FeCl_2{\cdot}4H_2O$ was added and deoxygenated by bubbling with nitrogen gas for 15 min, followed by heating to 80 °C. Then $N_2H_4{\cdot}H_2O$ (600 μl, 20 wt%) was added rapidly to the heated solution, which was left to stir for another 1 h. After cooling to room temperature, the formed G/Fe_3O_4 nanocomposites were isolated with the help of a magnet field and thoroughly washed by deionized water. The G/Fe_3O_4 nanocomposites were dry in vacuum for further characterization and application. The three samples (sample A, sample B, sample C) were prepared by change the addition amount of $FeCl_3{\cdot}6H_2O$ (0.2 mmol, 0.1 mmol, 0.04 mmol) and $FeCl_2{\cdot}4H_2O$ (0.1 mmol, 0.05 mmol, 0.02 mmol). The related information of the three samples are shown in Table 1. The Fe_3O_4 NCs were prepared by the same procedure without addition of GO.

2.4. Adsorption experiments

The removal of the organic dye from aqueous solutions by the G/Fe_3O_4 nanocomposite was carried out using following experimental procedures: a known amount of magnetic graphene nanocomposite was added to 20 ml of dye solutions with the concentration 0.02 mg ml^{-1}. After 1 h, the magnetic graphene nanocomposite was removed from the solution by magnetic separation using permanent magnet and the equilibrium concentration of the dyes in the solution was determined with UV–vis spectrophotometer at the wavelength of 554 nm (λ_{max}). The removed quantity (q_{eq} in mg g^{-1}) of the dye by the magnetic graphene nanocomposite was calculated by the following expression:

$$q_{eq} = \frac{C_0 - C_{eq}}{m} V \quad (1)$$

where C_0 (mg l^{-1}) represents the initial dye concentration, C_{eq} (mg l^{-1}) is the equilibrium concentration of the dye remaining in the solution, V (l) is the volume of the aqueous solution, and m (g) is the weight of the G/Fe_3O_4 nanocomposite.

3. Results and discussion

3.1. X-ray diffraction (XRD) analysis

Fig. 1 exhibits the XRD results of the as-synthesized Fe_3O_4, GO and G/Fe_3O_4. The GO presents a very sharp diffraction peak at 10.3°, which indicates that the (0 0 2) inter-planar spacing increased due to the oxide treatment, whereas the weak and broad peak between 20 and 30° suggests residual unoxidized graphite. For Fe_3O_4 and G/Fe_3O_4 (samples A–C), the position of all significant diffraction peaks matched well with data from the JCPDS card for Fe_3O_4 and can be assigned to the (2 2 0), (3 1 1), (4 0 0), (4 2 2), (5 1 1), and (4 4 0) of crystal planes of Fe_3O_4.

3.2. Transmission electron microscopy (TEM) analysis

The formation of Fe_3O_4 decorated graphene sheets is further confirmed by TEM observation. The morphology and microstructure of as-synthesized G/Fe_3O_4 nanocomposites were examined by TEM as shown in Fig. 2. From Fig. 2(a)–(f), the hybrid structures of samples A–C with different magnification were presented. It is evident that for all three samples, nanosized Fe_3O_4 particles anchored on graphene uniformly. Except the Fe_3O_4 particles decorated on graphene nanosheet, there are no other particles can be observed, which indicates the well combination between graphene and Fe_3O_4 NCs. From TEM images, a tendency that the sizes of Fe_3O_4 NCs decrease with increasing GO ratio in hybrids could be observed clearly. The average sizes of Fe_3O_4 NCs in three samples decrease from 24 nm to 13 nm, and 6 nm with the

Table 1
Parameters for the three samples.

Sample	Weight ratio (GO/Fe_3O_4)	Average size	Efficiency	Saturation magnetization
A	1:5.0	24 nm	96.7%	42.90 emu/g
B	1:2.5	13 nm	98.9%	29.88 emu/g
C	1:1.0	6 nm	99.2%	13.19 emu/g

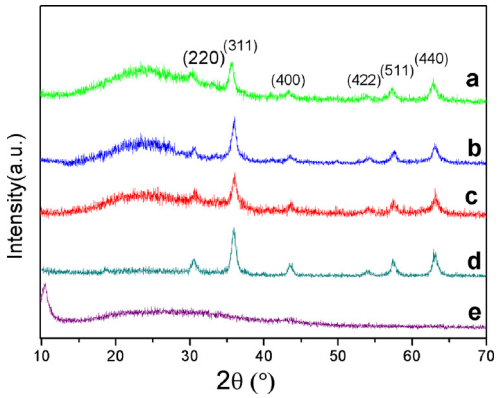

Fig. 1. XRD patterns of sample A (a), sample B (b), sample C (c), pure Fe_3O_4 NCs (d), and GO (e).

increasing ratio of GO to Fe_3O_4, which will induce the different coverage fraction of graphene sheet by Fe_3O_4 NCs. Since the mechanism of the G/Fe_3O_4 adsorption of the organic dye may be derived from two reasons: one reason might be based on van der Waals interactions occurring between the hexagonally arrayed carbon atoms in the graphite sheet of G/Fe_3O_4 and the aromatic backbones of the dye; the second reason might be due to the strong π-stacking interaction between the benzene ring of the dye and the large delocalized π-electron system of the G [31], the different sizes of Fe_3O_4 NCs will affect the extraction efficiency of organic dye from wastewater. Therefore, the treatment effectiveness of wastewater using the organic dye Rh.B as the adsorbate by the three samples is investigated. Because one of merits of G/Fe_3O_4 hybrid for wastewater treatment is convenient separation by magnetic field, the magnetic properties of the three samples should be clarified before adsorption experiment.

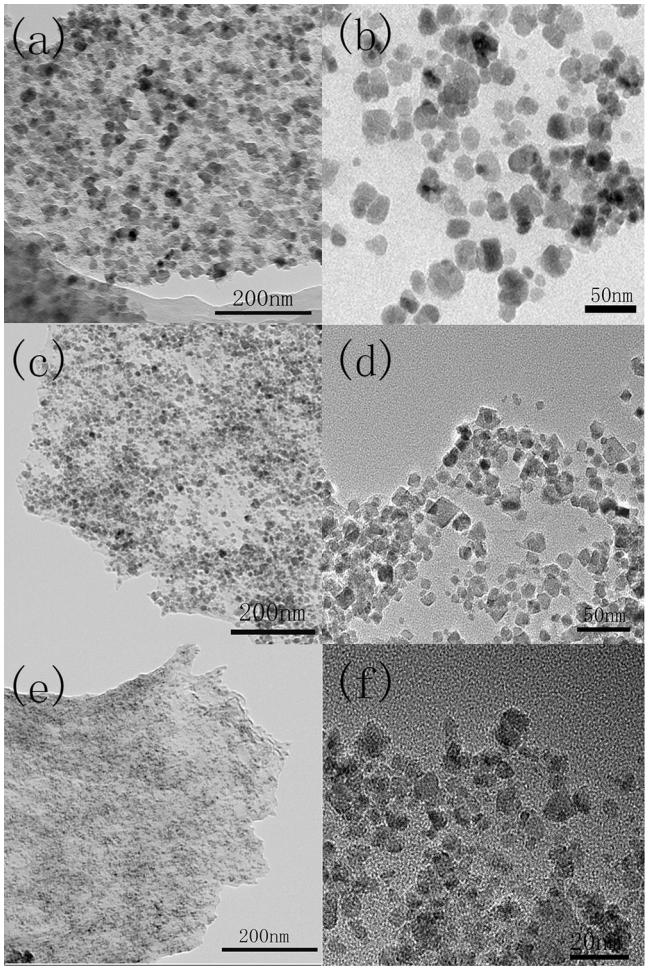

Fig. 2. (a) and (b) are TEM images of sample A taken under different magnification; (c) and (d) are that of sample B; (e) and (f) are that of sample C.

3.3. Vibrating sample magnetometer (VSM) analysis

The magnetic properties of the synthesized products are shown in Fig. 3 and shows that the magnetic properties are sensitive to the crystal sizes. The saturation magnetization (*Ms*) values of the samples are smaller than those of the bulk materials (92 emu/g). The particle size has been reported to influence the magnetic properties of materials [32,33]. The saturation magnetization of all the samples increases from 13.19 to 29.88 to 42.9, and 51.8 emu/g at 16 kOe with decreasing GO ratio, which can be attributed to the growth of particle size, enhancement in crystallinity, and reduction of surface adsorbed species. The decrease of the saturation magnetization of all the samples than the bulk magnetite is often observed with the NCs and is most likely attributed to the existence of organic coating agents [34]. Some studies suggested that the presence of the coating agents decreases the uniformity due to quenching of surface moments, resulting in the reduction of magnetic moment in such NCs [35]. The inset image shown in the bottom right inset of Fig. 3 shows the separation of G/Fe_3O_4 (sample C) from aqueous solution, a total of 10 ml of a 2 mg ml^{-1} G/Fe_3O_4 aqueous dispersion was separated under an external magnetic field and get a clear aqueous media.

3.4. Adsorption of Rh.B with G/Fe_3O_4

Fig. 4 describes the concentration variation of Rh.B as a function of loading amount of the three samples. It was observed that the percentages of the dye adsorbed increased as the G/Fe_3O_4 dosage was increased over the range from 4 to 15 mg and the removal ratio gets to saturation when the loading amount of G/Fe_3O_4 is more than 15 mg. The maximum removal ratio of the dye for samples A, B, and C are 96.7%, 98.9% and 99.2%, respectively. Fig. 5 shows the effect of adsorption time on the removal ratio of Rh.B (at initial concentration of 20 mg ml^{-1}) with 15 mg loading amount for all three samples. A fast adsorption process of Rh.B occurred during the first few minutes and the adsorbed amount of Rh.B reached

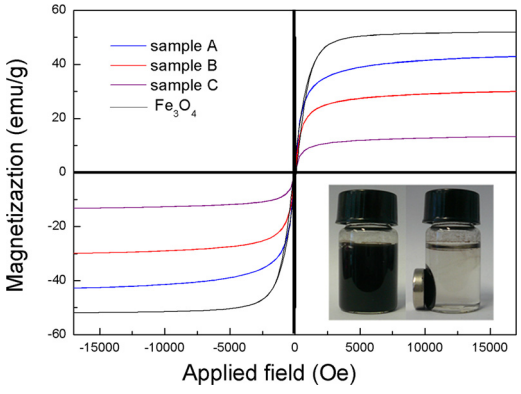

Fig. 3. VSM magnetization curves of the three G/Fe_3O_4 samples and Fe_3O_4 NCs. The inset shows the separation of G/Fe_3O_4 (sample C) from aqueous solution under an external magnetic field.

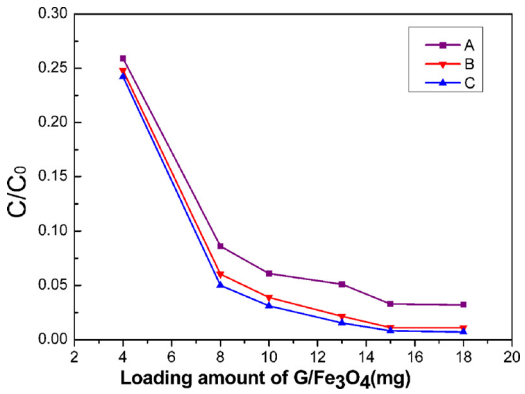

Fig. 4. The concentration of remnant Rh.B as a function of loading amount of the three samples after stirring 1 h.

equilibrium value quickly. The equilibrium time was about 25 min. For sample C, about 96.3% of the dye was adsorbed within 10 min and 98.3% of the dye was adsorbed within 25 min. The inset exhibits adsorption characteristics of sample C. After stirring the mixture of G/Fe_3O_4 and Rh.B aqueous solution (right) for 30 min, the supernatant turned nearly colorless (left) and the G/Fe_3O_4 nanocomposites can be separated from the aqueous solution by a permanent magnet. As shown in Table 1, the removal ratio of dye increases with increasing ratio of GO to Fe_3O_4, which is consistent with adsorption mechanism discussed above. The high extraction efficiency of the G/Fe_3O_4 is attributed to the large surface area and high adsorption ability of graphene sheet. The coverage fraction of graphene sheet decreases from sample A to sample C so that more dye molecules could be adsorbed by graphene sheet of sample C. According to the experimental results, the magnetization of Fe_3O_4 NCs will decreases with the decreasing sizes of Fe_3O_4 NCs, but the maximum removal ratio of the dye will increases with the decreasing sizes of Fe_3O_4 NCs. One problem here is that the separation of G/Fe_3O_4 from wastewater after reaching equilibrium value will take more time with the decreasing sizes of Fe_3O_4 NCs under the same magnetic field since the magnetization will decreases. For example, the separation time of sample A from wastewater is less than 1 min, and that of sample C will take 10 min in our experiments. Therefore, how to balance the removal efficiency and the separation time should be still considered for practical application.

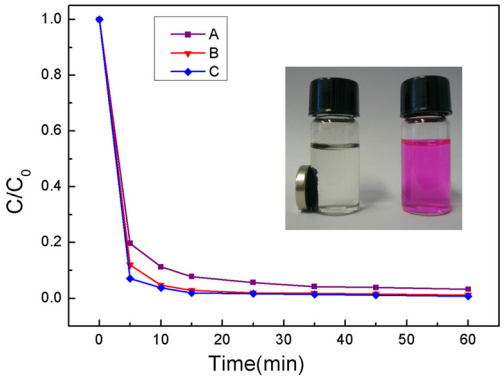

Fig. 5. Effect of adsorption time on the removal ratio of the Rh.B of the three samples in water with 15 mg loading amount. The inset exhibits adsorption characteristics of sample C. After stirring the mixture of G/Fe_3O_4 and Rh.B aqueous solution (right) for 30 min, the supernatant turned nearly colorless (left) and the G/Fe_3O_4 nanocomposites can be separated from the aqueous solution by a permanent magnet.

3.5. Adsorption kinetic and isotherms analysis

A study of adsorption kinetic is expected as it can provide information of the mechanism of adsorption. The pseudo-first-order and pseudo-second-order models were employed to investigate the kinetics of adsorption of Rh.B on the three samples. The pseudo-first-order kinetic model is expressed by following equation:

$$\frac{1}{q_t} = \frac{k_1}{q_e t} + \frac{1}{q_e} \tag{2}$$

where q_t (mg/g) is the amount adsorbed at time t (min). k_1 is the first-order rate constant, q_t (mg g^{-1}) and q_e(mg g^{-1}) represent the amount of the dye adsorbed at any time t (min) and at equilibrium, respectively. The fitting results are shown in Fig. 6.

The pseudo-second-order kinetic model is expressed as:

$$\frac{t}{q_t} = \frac{1}{k_2 q_e^2} + \frac{1}{q_e} t \tag{3}$$

where k_2 (g mg^{-1} min^{-1}) is the second-order rate constant, q_t (mg g^{-1}) and q_e (mg g^{-1}) represent the amount of the dye adsorbed at any time t (min) and at equilibrium, respectively. The fitting results are shown in Fig. 7. The parameters obtained from different kinetic models at common initial concentration of Rh.B (20 mg/l) are presented in Table 2. The values of coefficient (R^2) of the pseudo-second-order kinetic model were greater than 0.99 for all samples which indicate the applicability of the pseudo-second-order model to describe the adsorption process. Based on the assumption of the pseudo-second-order kinetic model [36], it can be concluded from the experimental result that the adsorption of Rh.B on G/Fe_3O_4 is due to a chemical adsorption.

The adsorption isotherms indicate the distribution of adsorbed molecules between the solid and liquid phase when the adsorption reach the equilibrium. The most common isotherm models are Langmuir and Freundlich isotherms [37,38]. In the study, the adsorption of Rh.B with different initial concentration was studied with an adsorption time t = 1 h, and temperature T = 298 K. The Langmuir isotherm model assumes that a monolayer adsorption exists on the adsorbent surface with a finite number of identical sites, that a site can only by occupied by one pollutant molecule and that there is no interaction between the adsorbed molecules. The Langmuir isotherm model is expressed by the following equation:

$$q_e = \frac{k q_m c_e}{1 + k c_e} \tag{4}$$

where q_e (mg/g) is the amount of adsorbed per unit weight of adsorbent, C_e is the equilibrium concentration of the adsorbate

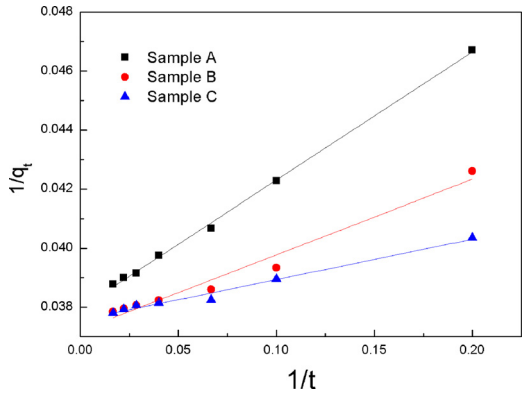

Fig. 6. Pseudo-first-order kinetic plot for adsorption of Rh.B onto three samples.

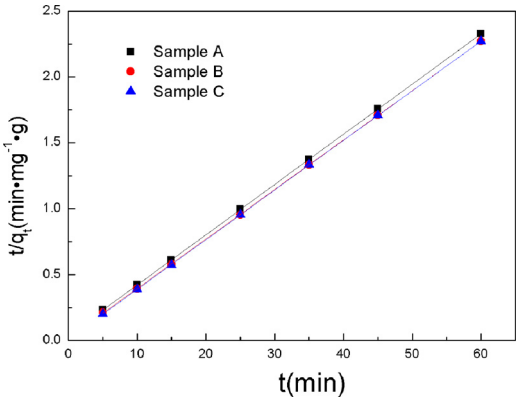

Fig. 7. Pseudo-second-order kinetic plot for adsorption of Rh.B onto three samples.

Table 2
Parameters obtained from different kinetic models.

Sample	Pesudo-first-order			Pesudo-second-order		
	q_e (mg/g)	k_1(L min^{-1})	R^2	q_e (mg/g)	k_2(g mg^{-1} min^{-1})	R^2
A	26.337	1.143	0.9986	26.267	28.537	0.9999
B	26.87	0.687	0.9687	26.674	14.436	0.9998
C	26.62	0.364	0.9819	26.582	9.115	0.9999

(mg/l), q_m is the maximum adsorption capacity (mg/g), and k (l/mg) is the constant that relates to the adsorption energy.

The Freundlich expression is an empirical equation based on adsorption on a heterogeneous surface. It has the following form:

$$q_e = k_F C_e^{1/n} \quad (5)$$

where k_F and $1/n$ are the Freundlich characteristic constants. The Freundlich constant ($1/n$) is related to the sorption intensity of the sorbent. When $0.1 < 1/n \leq 0.5$, it is easy to adsorb; if $0.5 < 1/n \leq 1$, there are some difficulties with the absorption; if $1/n > 1$, it is quite difficult to adsorb [39].

The theoretical plots from Langmuir and Freundlich isotherm and the experimental data for adsorption of Rh.B on adsorbent are shown in Fig. 8. For Langmuir isotherm, the order of the maximum adsorption capacity q_m of different adsorbents in our experiments is sample C > sample B > Sample A. The Langmuir and Freundlich parameters and calculated coefficients are listed in Table 3. From Table 3, the Langmuir isotherm model yielded better fitting than

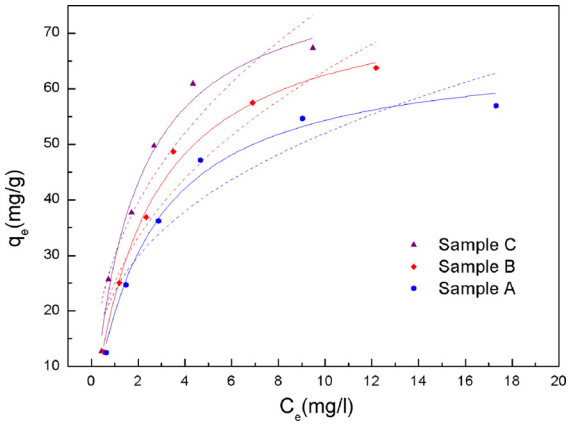

Fig. 8. Adsorption isotherms of Rh.B on three samples. Solid lines represent Langmuir model fitting and dashed lines represent Freundlich model fitting.

Table 3
Paramenters for Langmuir and Freundlich isotherm models.

Sample	Langmuir model			Freundlich model		
	q_m (mg/g)	k (L/mg)	R^2	K_F ((mg^{1-n} L^n)/g)	$1/n$	R^2
A	67.43	0.414	0.985	23.53	0.344	0.858
B	77.66	0.41	0.992	25.19	0.399	0.914
C	82.41	0.547	0.983	30.04	0.396	0.892

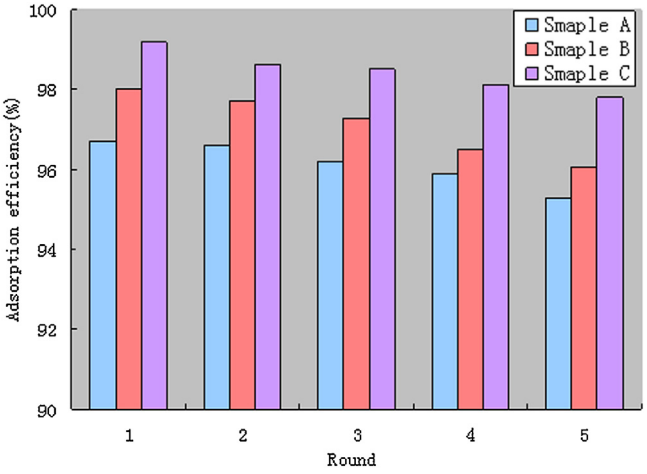

Fig. 9. Cycling runs in the extraction of Rh.B with the three samples.

the Freundlich model, which suggests monolayer coverage of Rh.B on G/Fe_3O_4 is the main mechanism.

3.6. Desorption and reused of adsorbents

The recycling and regeneration ability is significant for the practical application of adsorbents. Therefore, the recycling of G/Fe_3O_4 in the removal of Rh.B was investigated. After adsorption, desorption was carried out by washing out G/Fe_3O_4 bound Rh.B with acidic ethanol (the pH value was adjusted to 3 by hydrochloric acid) [40] and by rinsing GO/Fe_3O_4 with Milli-Q water; then, G/$Fe_3O_4$was separated by magnet and reused. The adsorbed Rh.B molecules could be efficiently desorbed. Fig. 9 shows the removal ratio of Rh.B of the three samples as a function of cycling runs. For sample C, the removal ratio after 1 h were 99.2%, 98.6%, 98.5%, 98.1% and 97.8%, respectively for the consecutive 5 cycling runs. The decline in efficiencies of all three samples is not more than 1.5% after recycle for five times, indicating that G/Fe_3O_4 has a good reusability. The repeated availability is an important factor for an advanced sorbent. The slightly decrease in efficiency is partly caused by the inevitable loss of the sorbents during washing process.

4. Conclusion

In summary, the effect of the stoichiometry of G/Fe_3O_4 nanocomposites prepared by a simple one-pot synthesis on efficiency of wastewater treatment was investigated. The loading amount of Fe_3O_4 nanoparticles has a great influence on adsorption performance. The increasing of weight ratio of GO to Fe_3O_4 reduced the sizes of Fe_3O_4 NCs, which induced smaller coverage fraction of graphene sheet so that the removal efficiency of organic dyes was improved. In addition, the adsorption capacity of the best composites in this work reached 83 mg/g. This research indicates

that G/Fe_3O_4 can be used as an effective sorbent for the simple and rapid removal of organic pollutants from water samples.

Acknowledgements

Financial support from the National Natural Science Foundation of China (authorization numbers: 61376020), Science and Technology Department of Jilin Province (20130101009JC,20140414024GH), Education Department of Jilin Province (2014116), China are acknowledged.

References

[1] K.S. Novoselov, A.K. Geim, S.V. Morozov, D. Jiang, Y. Zhang, S.V. Dubonos, I.V. Grigorieva, A.A. Firsov, Electric field effect in atomically thin carbon films, Science 306 (2004) 666–669.
[2] K.S. Kim, Y. Zhao, H. Jang, S.Y. Lee, J.M. Kim, K.S. Kim, J.H. Ahn, P. Kim, J.Y. Choi, B. H. Hong, Large-scale pattern growth of graphene films for stretchable transparent electrodes, Nature 457 (2009) 706–710.
[3] S. Stankovich, D.A. Dikin, G.H.B. Dommett, K.M. Kohlhaas, E.J. Zimney, E.A. Stach, R.D. Piner, S.T. Nguyen, R.S. Ruoff, Graphene-based composite materials, Nature 442 (2006) 282–286.
[4] W. Xue, R. Zhao, X. Du, F. XU, Graphene–Fe_3O_4 micro–nano scaled hybrid spheres: synthesis and synergistic electromagnetic effect, Mater. Res. Bull. 50 (2014) 285–291.
[5] T. Nakajima, Y. Matsuo, Formation process and structure of graphite oxide, Carbon 32 (1994) 469–475.
[6] M.D. Stoller, S.J. Park, Y.W. Zhu, J.H. An, R.S. Ruoff, Graphene-based ultracapacitors, Nano Lett. 8 (2008) 3498–3502.
[7] L.L. Zhang, H.H. Cheng, H.M. Zhang, L.T. Qu, Direct electrochemistry and electrocatalysis of horseradish peroxidase immobilized in graphene oxide–nafion nanocomposite film, Electrochim. Acta 65 (2012) 122–126.
[8] C. Basavaraja, W.J. Kim, Y.D. Kim, D.S. Huh, Synthesis of polyaniline-gold/graphene oxide composite and microwave absorption characteristics of the composite films, Mater. Lett. 65 (2011) 3120–3123.
[9] L. Gu, X. He, Z. Wu, Mesoporous Fe_3O_4/hydroxyapatite composite for targeted drug delivery, Mater. Res. Bull. 59 (2014) 65–68.
[10] S. Chen, J.W. Zhu, X.D. Wu, Q.F. Han, X. Wang, Graphene oxide-MnO_2 nanocomposites for supercapacitors, ACS Nano 4 (2010) 2822–2830.
[11] A.R. Marlinda, N.M. Huang, M.R. Muhamad, M.N. Anamt, B.Y.S. Chang, N. Yusoff, I. Harrison, H.N. Lim, C.H. Chia, S.V. Kumar, Highly efficient preparation of ZnO nanorods decorated reduced graphene oxide nanocomposites, Mater. Lett. 80 (2012) 9–12.
[12] H.J. Song, X.H. Jia, N. Li, X.F. Yang, H. Tang, Synthesis of α-Fe_2O_3 nanorod/graphene oxide composites and their tribological properties, J. Mater. Chem. 22 (2012) 895–902.
[13] J.S. Zhou, L.L. Ma, H.H. Song, B. Wu, X.H. Chen, Durable high-rate performance of CuO hollow nanoparticles/graphene-nanosheet composite anode material for lithium-ion batteries, Electrochem. Commun. 13 (2011) 1357–1360.
[14] J. Liu, X. Pu, D. Zhang, Combustion synthesis of CdS/reduced graphene oxide composites and their photocatalytic properties, Mater. Res. Bull. 57 (2014) 29–34.
[15] T. Wang, Z. Liu, M. Lu, B. Wen, et al., Graphene–Fe_3O_4 nanohybrids: synthesis and excellent electromagnetic absorption properties, J. Appl. Phys. 113 (2013) 024314.
[16] M. Zhang, M. Jia, Y. Jin, Fe_3O_4/reduced graphene oxide nanocomposite as high performance anode for lithium ion batteries, Appl. Surf. Sci. 261 (2012) 298–305.
[17] J.Z. Wang, C. Zhong, D. Wexler, N.H. Idris, Z.X. Wang, L.Q. Chen, Graphene-encapsulated Fe_3O_4 nanoparticles with 3d laminated structure as superior anode in lithium ion batteries, Chem. Eur. J. 17 (2011) 661–667.
[18] C. Ataca, E. Akturk, S. Ciraci, H. Ustunel, High-capacity hydrogen storage by metallized graphene, Appl. Phys. Lett. 93 (2008) 43123.
[19] K. Dutta, S. Mukhopadhyaya, S. Bhattacharjee, B. Chaudhuri, Chemical oxidation of methylene blue using a Fenton-like reaction, J. Hazard. Mater. 84 (2001) 57–71.
[20] G. Capar, U. Yetis, L. Yilmaz, Membrane based strategies for the pre-treatment of acid dye bath wastewaters, J. Hazard. Mater. 135 (2006) 423–430.
[21] C.H. Liu, J.S. Wu, H.C. Chiu, S.Y. Suen, K.H. Chu, Removal of anionic reactive dyes from water using anion exchange membranes as adsorbers, Water Res. 41 (2007) 1491–1500.
[22] M. Muruganandham, M. Swaminathan, TiO_2–UV photocatalytic oxidation of reactive yellow 14: effect of operational parameters, J. Hazard. Mater. 135 (2006) 78–86.
[23] E. Guibal, M. Van Vooren, B. Dempsey, J. Roussy, A review of the use of chitosan for the removal of particulate and dissolved contaminants, Sep. Sci. Technol. 41 (2006) 2487–2514.
[24] Y. Zhan, F. Meng, Y. Lei, R. Zhao, J. Zhong, X. Liu, One-pot solvothermal synthesis of sandwich-like graphene nanosheets/Fe_3O_4 hybrid material and its microwave electromagnetic properties, Mater. Lett. 65 (2011) 1737–1740.
[25] K. Zhou, Y. Zhu, X. Yang, C. Li, One-pot preparation of graphene/Fe_3O_4 composites by a solvothermal reaction, New J. Chem. 34 (2010) 2950–2955.
[26] X. Shen, J. Wu, S. Bai, H. Zhou, One-pot solvothermal syntheses and magnetic properties of graphene-based magnetic nanocomposites, J. Alloys. Compd. 506 (2010) 136–140.
[27] P.S. Teo, H.N. Lim, N.M. Huang, C.H. Chia, I. Harrison, Room temperature in situ chemical synthesis of Fe_3O_4/graphene, Ceramic Int. 38 (2012) 6411–6416.
[28] Y. He, Q. Sheng, J. Zheng, M. Wang, B. Liu, Magnetite-graphene for the direct electrochemistry of hemoglobin and its biosensing application, Electrochim. Acta 56 (2011) 2471–2476.
[29] Q.X. Zhang, Q.Q. Ren, Y.Q. Miao, J.H. Yuan, K.K. Wang, F.H. Li, D.X. Han, L. Niu, One-step synthesis of graphene/polyallylamine-Au nanocomposites and their electrocatalysis toward oxygen reduction, Talanta 89 (2012) 391–395.
[30] W. Lü, Y. Wu, J. Chen, Y. Yang, Facile preparation of graphene–Fe_3O_4 nanocomposites for extraction of dye from aqueous solution, CrystEngComm 16 (2014) 609–615.
[31] Q. Wu, C. Feng, C. Wang, Z. Wang, A facile one-pot solvothermal method to produce superparamagnetic graphene-Fe_3O_4 nanocomposite and its application in the removal of dye from aqueous solution, Colloids Surf. B 101 (2013) 210–214.
[32] R.H. Kodama, A.E. Berkowitz, E.J. McNiff Jr., S. Foner, Surface spin disorder in $NiFe_2O_4$ nanoparticles, Phys. Rev. Lett. 77 (1996) 394–397.
[33] L. Rezlescu, E. Rezlescu, P.D. Popa, N. Rezlescu, Fine barium hexaferrite powder prepared by the crystallisation of glass, J. Magn. Magn. Mater. 193 (1999) 288–290.
[34] G.F. Goya, T.S. Berquo, F.C. Fonseca, M.P. Morales, Static and dynamic magnetic properties of spherical magnetite nanoparticles, J. Appl. Phys. 94 (2003) 3520–3528.
[35] D.K. Kim, M. Mikhaylova, Y. Zhang, M. Muhammed, Protective coating of superparamagnetic iron oxide nanoparticles, Chem. Mater 15 (2003) 1617–1627.
[36] V. Vadivelan, K.V. Kumar, Equilibrium, kinetics, mechanism, and process design for the sorption of methylene blue onto rice husk, J. Colloid Interface Sci. 286 (2005) 90.
[37] I. Langmuir, Adsorption of gases on plain surface of glass mica platinum, J. Am. Chem. Soc. 40 (1918) 136–403.
[38] H.M.F. Freundlich, Over the adsorption in solution, J. Phys. Chem. 57 (1906) 385–470.
[39] T.H. Liu, Y.H. Li, Q.J. Du, J.K. Sun, Y.Q. Jiao, G.M. Yang, Z.H. Wang, Y.X. Xia, K.L. Wang, H.W. Zhu, D.H. Wu, Adsorption of methylene blue from aqueous solution by graphene, Colloids Surf. B 90 (2012) 197–201.
[40] J. Gong, B. Wang, G. Zeng, C. Yang, C. Niu, Q. Niu, W. Zhou, Y. Liang, Removal of cationic dyes from aqueous solution using magnetic multi-wall carbon nanotube nanocomposite as adsorbent, J. Hazard. Mater. 164 (2009) 1517–1522.